Hindawi Publishing Corporation
Advances in Condensed Matter Physics
Volume 2013, Article ID 673945, 5 pages
http://dx.doi.org/10.1155/2013/673945

Research Article

A Facile Synthesis and Optical Properties of Bundle-Shaped $TbPO_4 \cdot H_2O$ Nanorods

Dan Yue,[1,2] Wen Luo,[2] Wei Lu,[3] Ruiyong Wang,[1] Chunyang Li,[2] Jiazhong Chang,[2] and Zhenling Wang[2]

[1] *The College of Chemistry and Molecular Engineering, Zhengzhou University, Zhengzhou 450001, China*
[2] *The Key Laboratory of Rare Earth Functional Materials and Applications, Zhoukou Normal University, Zhoukou 466001, China*
[3] *Department of Applied Physics and Materials Research Center, The Hong Kong Polytechnic University, Hong Kong*

Correspondence should be addressed to Ruiyong Wang; wangry@zzu.edu.cn and Zhenling Wang; wangzhenling@zknu.edu.cn

Received 14 November 2013; Accepted 1 December 2013

Academic Editor: Jianhua Hao

Bundle-shaped $TbPO_4 \cdot H_2O$ nanorods have been prepared by a facile hydrothermal technique and characterized by XRD, SEM, TEM, UV-Vis diffuse reflectance spectrum (DRS), photoluminescence (PL) spectrum, and lifetime. The results indicate that the obtained sample has hexagonal structure of $TbPO_4 \cdot H_2O$ and is composed of nanorods bundles which is assembled from many single crystalline nanorods with the diameter of around 45 nm and the length of 2.3 μm. The growth of the single crystalline nanorod is along the (001) plane direction. Under the UV light irradiation, $TbPO_4 \cdot H_2O$ nanorods bundles exhibit bright green emission corresponding to the $^5D_4 \rightarrow {}^7F_J$ ($J = 6, 5, 4, 3$) transitions of the Tb^{3+} ions, and the lifetime is determined to be about 0.24 ms.

1. Introduction

In recent years, inorganic nanostructures with well-defined shapes and sizes have attracted growing attention because of their unique size- and shape-dependent properties [1–3]. Among many kinds of nanostructured materials, lanthanide orthophosphates ($LnPO_4$) with uniform size and various morphologies have been prepared by some mild and controllable methods [4, 5] and attracted great interest because of their unique properties including very low solubility in water (The solubility product constant, $pK_{sol} = 25$–27) [6], high thermal stability, high index of refraction, and high luminescent efficiency [7, 8]. These materials have been used as active components in a wide range of applications such as phosphors, laser hosts, and biolabeling [9–12]. The chemical and optical properties of one-dimensional (1D) $LnPO_4$ nanostructures (e.g., $CePO_4 : Tb^{3+}$ nanowires, $LaPO_4$ nanorods, $CePO_4$ peanut-liked nanostructures, etc.) can be successfully tailored, which makes these materials have significant potential applications in fabricating the next generation of information storage, optoelectronic, sensing devices, and nanoscale devices [13–15].

As an important sort of lanthanide phosphates, $TbPO_4$ has been investigated mainly focusing on its physical low-temperature properties (magnetic properties, birefringence measurements, and mean-field calculations) in previous literatures [16, 17]. Recently, much attention has been focused on the synthesis and properties of the $TbPO_4$ with various morphologies. It is known that the hydrothermal technique is a common method in the field of material science. Using this technique, many materials with uniform morphology and satisfying crystallinity can be obtained at relatively low reaction temperature, usually without any further calcinations at high temperature [18, 19]. For example, $TbPO_4 : Eu^{3+}$ square-like particles were prepared by hydrothermal method with citric acid as the organic additive, and the reaction temperature is as low as 160°C [20]. As a contrast, $TbPO_4$ hollow spheres can be obtained through solid state method when the annealing temperature is increased to 1150°C [21, 22]. In this work, uniform $TbPO_4 \cdot H_2O$ bundle-shaped nanostructures composed of single crystalline nanorods were synthesized at 180°C through a facile hydrothermal technique and characterized by XRD, SEM, TEM DRS, PL spectra, and so forth. The possible mechanism leading to

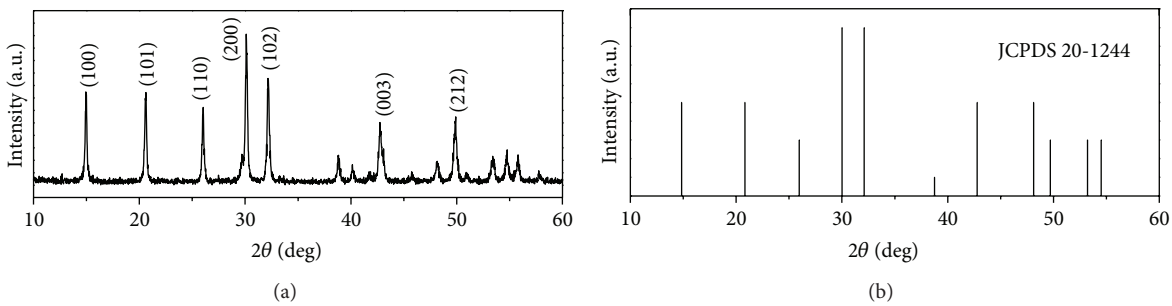

Figure 1: XRD patterns of bundle-shaped $TbPO_4 \cdot H_2O$ nanorods (a) and standard data of bulk $TbPO_4 \cdot H_2O$ ((b), JCPDS card 20-1244).

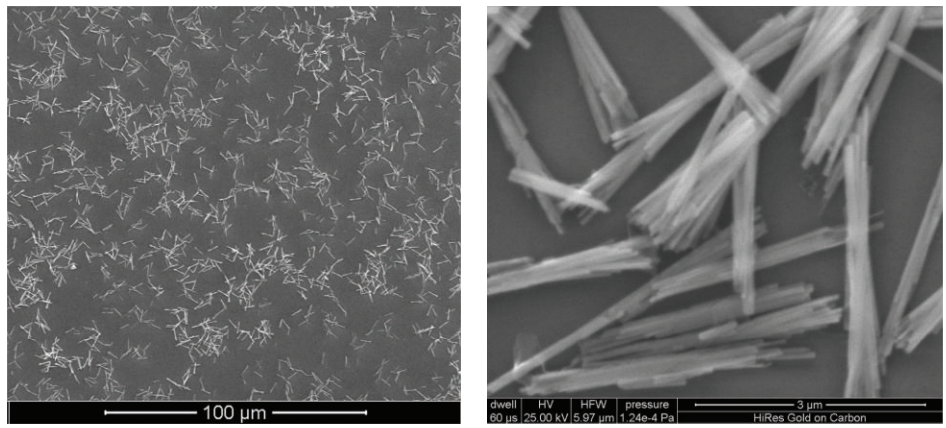

(a) (b)

Figure 2: SEM images (a) and (b) of $TbPO_4 \cdot H_2O$ nanorods bundles.

bundle-shaped structures, phase structure, morphology, and optical properties were discussed in detail.

2. Experimental Section

2.1. Synthesis of Bundle-Shaped $TbPO_4 \cdot H_2O$ Nanorods. Tb_4O_7 (99.99%) and $(NH_4)_2HPO_4$ (≥98.5%) were used as starting materials without any further purification. $Tb(NO_3)_3$ was prepared by dissolving Tb_4O_7 in diluted nitric acid, and the water in the solutions was distilled off by heating. Bundle-shaped $TbPO_4 \cdot H_2O$ nanorods were prepared by hydrothermal technique. Typically, 2 mmol of $(NH_4)_2HPO_4$ was added to 20 mL of 0.1 mol/L $Tb(NO_3)_3$ aqueous solution and the mixture was continuously stirred for 2 h. The obtained suspension was then transferred into a Teflon bottle held in a stainless steel autoclave, which was sealed and hydrothermally treated at 180°C for 24 h. After the autoclave was cooled to room temperature naturally, the precipitates were separated by centrifugation, washed with ethanol and distilled water twice, respectively, and dried at 70°C for 24 h to obtain the sample.

2.2. Characterization. Phase structure was characterized by a Bruker D8 Advance X-ray diffractometer (XRD) with Cu-Kα radiation (λ = 0.15406 nm). The accelerating voltage and emission current were 40 kV and 40 mA, respectively. Morphology of the samples was observed using a scanning electron microscope (SEM, Quanta 200) with an acceleration voltage of 25 kV. The TEM image and selected area electron diffraction (SAED) pattern were obtained on a JEOL-2010 transmission electron microscope at an accelerating voltage of 200 kV. UV-Vis diffuse reflectance spectrum (DRS) was obtained using a UV/Vis Spectrophotometer (Lambda35, PerkinElmer) equipped with an integrating sphere attachment. Photoluminescence (PL) spectra and lifetime were recorded using an FLS920P Edinburgh Analytical Instrument apparatus equipped with a 450 W xenon lamp and a μF900H high-energy microsecond flash lamp as the excitation sources.

3. Results and Discussion

3.1. Phase Structure and Morphology. Figure 1 shows the XRD patterns of bundle-shaped $TbPO_4 \cdot H_2O$ nanorods (Figure 1(a)) and standard data of $TbPO_4 \cdot H_2O$ powders (Figure 1(b)). It can be seen that all of the diffraction peaks of the bundle-shaped $TbPO_4 \cdot H_2O$ nanorods are in agreement with the standard data of hexagonal structure $TbPO_4 \cdot H_2O$ (JCPDS No. 20-1244), with the space group of $P3_121$ (152). Figures 2(a) and 2(b) show the low- and high-magnification SEM images of $TbPO_4 \cdot H_2O$ nanorods bundles, respectively. It can be seen that these bundle-shaped

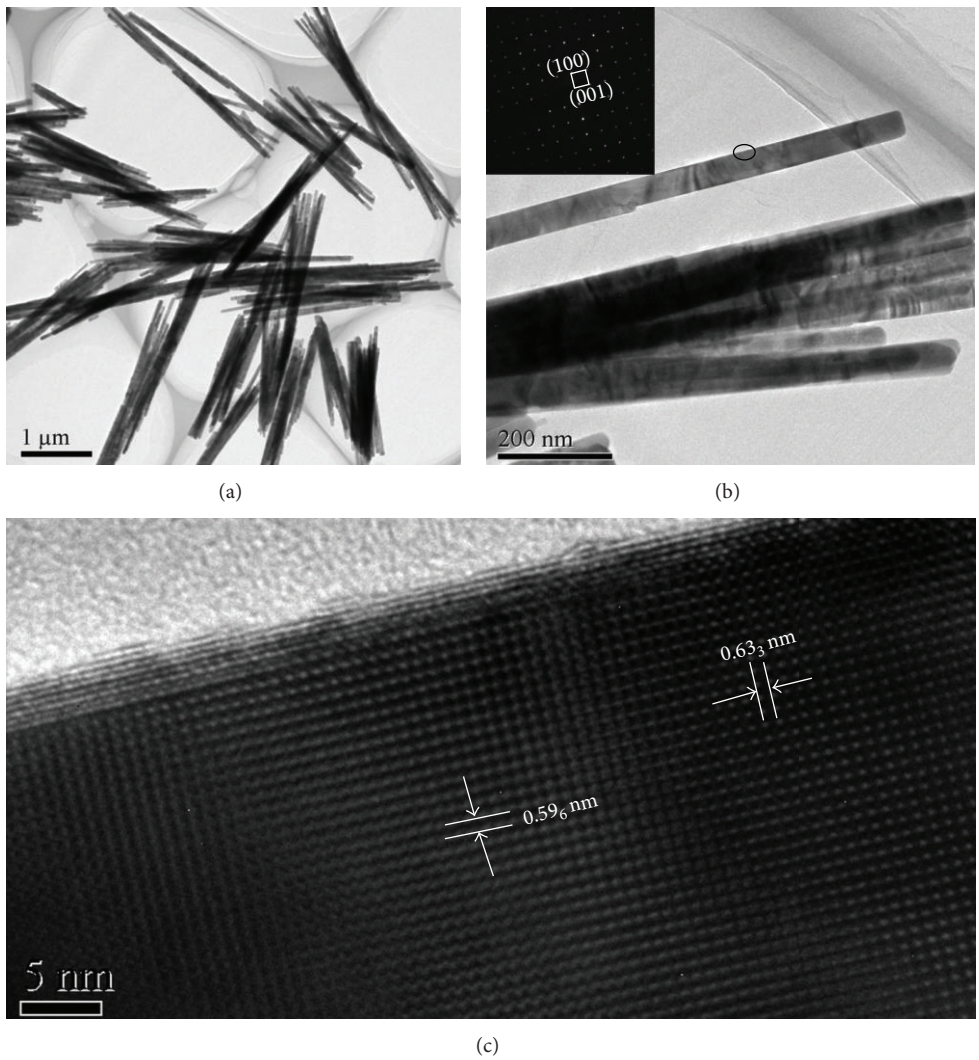

FIGURE 3: TEM images of bundle-shaped $TbPO_4 \cdot H_2O$ nanorods (a) and (b), SAED pattern (inset in (b)), and HRTEM image (c) of the single nanorod.

structures are homogeneous in the large field of vision (Figure 2(a)), the magnified image (Figure 2(b)) indicates that the bundle-shaped structures are actually composed of nanorods, and most of the nanorods are linked together by side-by-side conjunction.

To investigate the growth mechanism and microstructure of bundle-shaped structures in detail, the obtained sample was observed by the TEM and high resolution TEM (HRTEM) images equipped with selected area electron diffraction (SAED) pattern (Figure 3). It can be clearly seen from Figure 3(a) that the obtained sample is composed of bundle-shaped morphology, which is assembled by many $TbPO_4 \cdot H_2O$ nanorods with the diameter of ~45 nm and the length of ~2.3 μm. A high-magnified image of bundled nanorods (Figure 3(b)) indicates that these single crystalline nanorods as the primary construction unit are relatively uniform. The SAED pattern (Figure 3(b), inset) taken from the upper single nanorod can be indexed to the (100) and (001) planes of $TbPO_4 \cdot H_2O$ single crystalline with the hexagonal phase structure. These findings are consistent with the XRD result mentioned above. The HRTEM image (Figure 3(c)) of the single $TbPO_4 \cdot H_2O$ nanorod marked as an oval in Figure 3(b) displays singlecrystalline nature. The values of interplanar spacing of $TbPO_4 \cdot H_2O$ nanorod are 0.596 and 0.633 nm, which is identical to the (100) and (001) facet distance of bulk $TbPO_4 \cdot H_2O$ powders, respectively. It can be seen that the growth direction of $TbPO_4 \cdot H_2O$ single-crystalline nanorod is along (001) plane. According to the experimental results and analysis, the growth mechanism of $TbPO_4 \cdot H_2O$ nanorods bundles was proposed. Generally, $TbPO_4 \cdot H_2O$ tends to grow as 1D nanorods, which is possibly due to the 1D characteristics of the infinite linear chains of hexagonal-structured $TbPO_4$ [7]. And then, the surface energy of these nanorods may change under the hydrothermal process [23], so these nanorods aggregates might be assembled and grown along the same direction

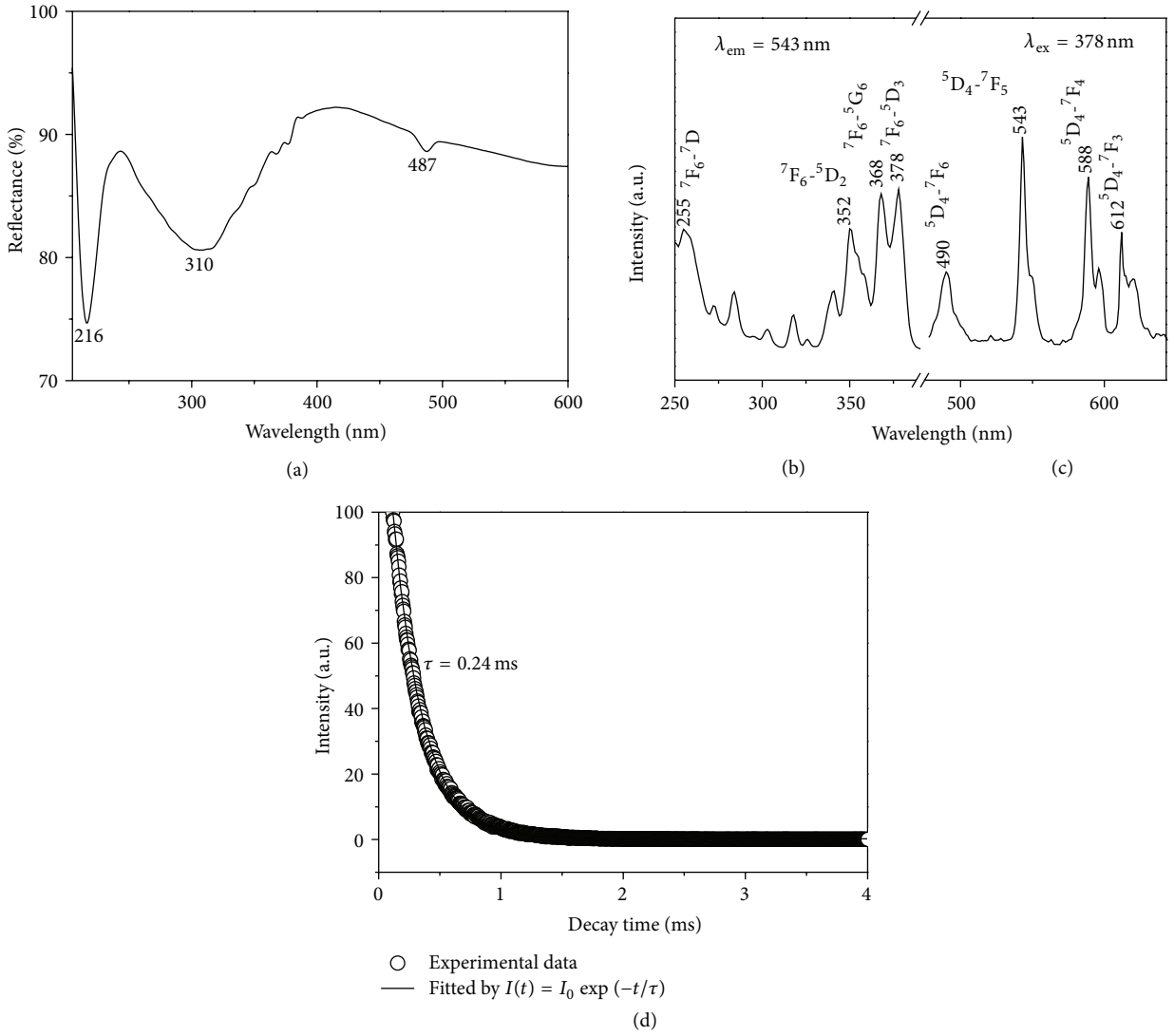

Figure 4: UV-Vis DRS (a), PL excitation (b), emission (c) spectra, and decay curve (d) of bundle-shaped $TbPO_4{\cdot}H_2O$ nanorods.

(oriented attachment) to form bundle-shaped structures. The formation process of $TbPO_4{\cdot}H_2O$ nanorods bundles is similar to that of $In(OH)_3$ rod bundles [24].

3.2. Optical Properties. Figure 4(a) shows the UV-Vis DRS spectrum of $TbPO_4{\cdot}H_2O$ nanorods bundles. The absorption peaks at 216 and 310 nm are due to the spin-allowed 4f-5d transition and the spin-forbidden transition of the Tb^{3+} ions, respectively. The absorption peak at 487 nm is assigned to the transitions from the ground level $^7F_6$ to the excited level $^5D_4$ of Tb^{3+} ion [25]. The excitation spectrum of $TbPO_4{\cdot}H_2O$ nanorods bundles was obtained by monitoring the emission of Tb^{3+} due to $^5D_4 \rightarrow {}^7F_5$ transition at 543 nm, as shown in Figure 4(b). It can be seen that the excitation peak at 255 nm is assigned to intra $4f^8$ transitions between the $4f^7 5d^1$, and most of the excitation peaks can be clearly assigned (352 nm: $^7F_6 \rightarrow {}^5D_2$; 368 nm: $^7F_6 \rightarrow {}^5G_6$; and 378 nm: $^7F_6 \rightarrow {}^5D_3$). Under the UV light irradiation (378 nm), the emission spectrum is composed of four well-resolved peaks at 490, 543, 588, and 612 nm, which is corresponding to the $^5D_4 \rightarrow {}^7F_J$ (J = 6, 5, 4, 3) transitions of Tb^{3+} ions as labeled in Figure 4(c). Figure 4(d) shows the PL decay curves of $TbPO_4{\cdot}H_2O$ nanorods bundles with the excitation wavelength (378 nm) and emission wavelength at 543 nm. The PL decay curve for Tb^{3+} in the $TbPO_4{\cdot}H_2O$ nanorods bundles can be well fitted into a single exponential function as $I(t) = I_0 \exp(-t/\tau)$ (τ is $1/e$ lifetime of Tb^{3+} ion) [26]. The lifetime for Tb^{3+} in $TbPO_4{\cdot}H_2O$ nanorods bundles is determined to be 0.24 ms.

4. Conclusion

In summary, the bundle-shaped $TbPO_4{\cdot}H_2O$ nanorods have been successfully prepared by the hydrothermal route. The reaction media are aqueous solution and free of any surfactants or templates, and the synthesis technique is simple and environmentally friendly. The bundle-shaped $TbPO_4{\cdot}H_2O$ nanostructures are assembled by many single crystalline $TbPO_4{\cdot}H_2O$ nanorods through side-by-side conjunction.

And these nanorods bundles yield green emission attributed to the transitions from the $^5D_4$ to the ^7F_J ($J = 6, 5, 4, 3$) energy levels of Tb^{3+}, which makes these nanorods bundles have potential applications in many fields such as lighting and optoelectronic devices with nanometer dimensions.

Acknowledgments

This work is financially supported by the National Natural Science Foundation of China (nos. 21171179 and 21301200), the Excellent Youth Foundation of He'nan Scientific Committee (134100510018), and the Program for Science & Technology Innovation Talents in University of Henan Province (no. 2011HASTIT030).

References

[1] G. Wang, Q. Peng, and Y. Li, "Lanthanide-doped nanocrystals: synthesis, optical-magnetic properties, and applications," *Accounts of Chemical Research*, vol. 44, no. 5, pp. 322–332, 2011.

[2] S. J. Zeng, M. K. Tsang, C. F. Chan, K. L. Wong, and J. H. Hao, "PEG modified $BaGdF_5$: Yb/Er nanoprobes for multi-modal upconversion fluorescent, in vivo X-ray computed tomography and biomagnetic imaging," *Biomaterials*, vol. 33, pp. 9232–9238, 2012.

[3] S. Zeng, J. Xiao, Q. Yang, and J. Hao, "Bi-functional NaLuF4: $Gd^{3+}/Yb^{3+}/Tm^{3+}$ nanocrystals: Structure controlled synthesis, near-infrared upconversion emission and tunable magnetic properties," *Journal of Materials Chemistry*, vol. 22, no. 19, pp. 9870–9874, 2012.

[4] C. X. Li, Z. Y. Hou, C. M. Zhang et al., "Controlled synthesis of Ln^{3+} (Ln= Tb, Eu, Dy) and V^{5+} ion-doped YPO_4 nano-/microstructures with tunable luminescent colors," *Chemistry of Materials*, vol. 21, no. 19, pp. 4598–4607, 2009.

[5] R. Komban, R. Beckmann, S. Rode et al., "Surface modification of luminescent lanthanide phosphate nanorods with cationic "quat-primer" polymers," *Langmuir*, vol. 27, no. 16, pp. 10174–10183, 2011.

[6] R. Yu, J. Bao, X. Yang et al., "Controlled synthesis of tetragonal terbium orthophosphate nanostructures through a solvothermal route," *Research on Chemical Intermediates*, vol. 37, no. 2-5, pp. 145–151, 2011.

[7] J. Bao, R. Yu, J. Zhang et al., "Controlled synthesis of terbium orthophosphate spindle-like hierarchical nanostructures with improved photoluminescence," *European Journal of Inorganic Chemistry*, no. 16, pp. 2388–2392, 2009.

[8] Y.-P. Fang, A.-W. Xu, R.-Q. Song et al., "Systematic synthesis and characterization of single-crystal lanthanide orthophosphate nanowires," *Journal of the American Chemical Society*, vol. 125, no. 51, pp. 16025–16034, 2003.

[9] W. Di, M.-G. Willinger, R. A. S. Ferreira, X. Ren, S. Lu, and N. Pinna, "Citric acid-assisted hydrothermal synthesis of luminescent TbPO 4:Eu nanocrystals: controlled morphology and tunable emission," *Journal of Physical Chemistry C*, vol. 112, no. 48, pp. 18815–18820, 2008.

[10] G. Phaomei, W. R. Singh, and R. S. Ningthoujam, "Solvent effect in monoclinic to hexagonal phase transformation in $LaPO_4$:RE (RE= Dy^{3+}, Sm^{3+}) nanoparticles: photoluminescence study," *Journal of Luminescence*, vol. 131, no. 6, pp. 1164–1171, 2011.

[11] M. Ferhi, K. Horchani-Naifer, and M. Férid, "Hydrothermal synthesis and photoluminescence of the monophosphate $LaPO_4$:Eu(5%)," *Journal of Luminescence*, vol. 128, no. 11, pp. 1777–1782, 2008.

[12] W. Bu, L. Zhang, Z. Hua, H. Chen, and J. Shi, "Synthesis and characterization of uniform spindle-shaped microarchitectures self-assembled from aligned single-crystalline nanowires of lanthanum phosphates," *Crystal Growth and Design*, vol. 7, no. 11, pp. 2305–2309, 2007.

[13] Y. Liu, Z.-G. Lu, Y.-Y. Gu, and W. Li, "Hydrothermal-assisted ion exchange synthesis and photoluminescence of Li^+ and Eu^{3+} co-doped $NaLa(WO_4)_2$ as near-UV type red phosphors," *Journal of Luminescence*, vol. 132, no. 5, pp. 1220–1225, 2012.

[14] Y.-F. Liu, Z.-P. Yang, and Q.-M. Yu, "Preparation and its luminescent properties of $AlPO_4$:Eu^{3+} phosphor for w-LED applications," *Journal of Alloys and Compounds*, vol. 509, no. 21, pp. L199–L202, 2011.

[15] C. Wu and Y. Wang, "Hydrothermal synthesis and luminescent properties of (La,Gd)PO_4:Tb phosphors under VUV excitation," *Materials Letters*, vol. 61, no. 11-12, pp. 2416–2418, 2007.

[16] P. Morin, J. Rouchy, and Z. Kazei, "Magnetic and magnetoelastic properties in tetragonal $TbPO_4$," *Physical Review B*, vol. 50, no. 17, pp. 12625–12634, 1994.

[17] C. Anderer, G. Hess, and H. G. Kahle, "Extensive studies on the low-temperature properties of $TbPO_4$. II. Measurements of the Faraday rotation," *Journal of Physics: Condensed Matter*, vol. 5, no. 7, article 022, pp. 945–954, 1993.

[18] Z. Wang, Z. Quan, and J. Lin, "Remarkable changes in the optical properties of CeO_2 nanocrystals induced by lanthanide ions doping," *Inorganic Chemistry*, vol. 46, no. 13, pp. 5237–5242, 2007.

[19] Z. L. Wang, J. H. Hao, H. L. W. Chan, W. T. Wong, and K. L. Wong, "A strategy to simultaneously realizing the cubic-to-hexagonal phase transition and controlling small size of $NaYF_4$:Yb^{3+}, Er^{3+} nanocrystals for in-vitro cell imaging," *Small*, vol. 8, no. 12, pp. 1863–1868, 2012.

[20] J. Lü, T. Fan, J. N. Xie, and G. J. Chen, "Tunable luminescence and energy transfer of $TbPO_4$:Eu^{3+} nanocrystals," *Optics Communications*, vol. 286, no. 12, pp. 221–223, 2013.

[21] L. H. Zhang, H. P. You, M. Yang, and Y. H. Song, "Facile one-pot synthesis and luminescence of hexagonal $TbPO_4 \cdot nH_2O$ hollow spheres," *Materials Letters*, vol. 67, no. 1, pp. 256–258, 2012.

[22] M. Yang, H. You, Y. Song et al., "Synthesis and luminescence properties of sheaflike $TbPO_4$ hierarchical architectures with different phase structures," *Journal of Physical Chemistry C*, vol. 113, no. 47, pp. 20173–20177, 2009.

[23] X. D. Zhang and Y. Xie, "Recent advances in free-standing two-dimensional crystals with atomic thickness: design, assembly and transfer strategies," *Chemical Society Reviews*, vol. 42, no. 21, pp. 8187–8199, 2013.

[24] J. Yang, C. Lin, Z. Wang, and J. Lin, "$In(OH)_3$ and In_2O_3 nanorod bundles and spheres: microemulsion-mediated hydrothermal synthesis and luminescence properties," *Inorganic Chemistry*, vol. 45, no. 22, pp. 8973–8979, 2006.

[25] Z.-L. Wang, H. L. W. Chan, H.-L. Li, and J. H. Hao, "Highly efficient low-voltage cathodoluminescence of LaF_3: Ln^{3+} (Ln= Eu^{3+}, Ce^{3+}, Tb^{3+}) spherical particles," *Applied Physics Letters*, vol. 93, no. 14, Article ID 141106, 2008.

[26] Z.-L. Wang, J. Hao, and H. L. W. Chan, "Light emission due to energy transfer from Gd^{3+} to Eu^{3+} ions in paramagnetic $NaGdF_4$: Eu^{3+} submicrometer disks," *Journal of the Electrochemical Society*, vol. 157, no. 10, pp. J315–J318, 2010.